

# Roundness and Sphericity of Soil Particles in Assemblies by Computational Geometry

Junxing Zheng, S.M.ASCE<sup>1</sup>; and Roman D. Hryciw, M.ASCE<sup>2</sup>

**Abstract:** The use of computational geometry methods for determining soil roundness ( $R$ ) and sphericity ( $S$ ) were evaluated and extended to particles segmented from images of three-dimensional particle assemblies. Two Adobe *Photoshop* lasso tools were used to delineate particles with full projections from the assemblies. Results were in excellent agreement with values published in traditional roundness and sphericity charts, thus confirming that the computational method can replace the much slower and less objective chart methods. Complete volume-based distributions of particle roundness and sphericity were presented for three soils with vastly different particle shapes. Values of  $R$  and  $S$  obtained from images of three-dimensional assemblies were almost indistinguishable from values obtained using images of detached particles showing their largest projected areas. Mean  $R$  values were also computed for 10 different soils of various geologic origins. As expected, crushed sands exhibited the smallest mean values of  $R$  whereas alluvial and glacio-fluvial soils showed the largest values. DOI: [10.1061/\(ASCE\)CP.1943-5487.0000578](https://doi.org/10.1061/(ASCE)CP.1943-5487.0000578). © 2016 American Society of Civil Engineers.

## Introduction

Soil particle form (shape) and roundness are intrinsic grain-level characteristics that, along with state parameters, control assembly level soil properties such as minimum and maximum void ratio, strength, compressibility, and shear wave velocity (Santamarina and Cho 2004; Cho et al. 2006; Bareither et al. 2008; Chapuis 2012; Shin and Santamarina 2013; Cabalar et al. 2013). However, the difficulties involved in determining particle form and roundness have impeded their application in practice. On the computational front, discrete element methods (DEMs) have shown great potential to simulate soil assembly behavior. However, in DEMs, soil particles are generally idealized as perfect spheres, and thus form and roundness effects must be accounted for in roundabout ways, for example, by artificially restricting particle rotations. Recently, DEM researchers have been developing the computational tools to simulate more realistic and complex particles. This will require more accurate and statistically valid quantification of the form and roundness of real soil particles.

Particle form is commonly quantified by a sphericity ( $S$ ) value. Various definitions have been proposed for this parameter. Almost all of the definitions are based on particle dimensions measured in images of two-dimensional (2D) projections of the particles (Tickell 1931; Wadell 1935; Krumbein and Sloss 1951; Santamarina and Cho 2004; Altuhafi et al. 2013). Computation of  $S$  by the various definitions can be readily automated by digital image analysis techniques (Kuo et al. 1996; Kuo and Freeman 2000; Rao and Tutumluer 2000; Fletcher et al. 2003; Kumara et al. 2012; Altuhafi et al. 2013 and others as surveyed by Hryciw et al. 2014).

<sup>1</sup>Graduate Student and Research Assistant, Dept. of Civil and Environmental Engineering, Univ. of Michigan, 2340 GG Brown, Ann Arbor, MI 48109-2125. E-mail: junxing@umich.edu

<sup>2</sup>Professor, Dept. of Civil and Environmental Engineering, Univ. of Michigan, 2366 GG Brown, Ann Arbor, MI 48109-2125 (corresponding author). E-mail: roman@umich.edu

Note. This manuscript was submitted on March 4, 2015; approved on December 22, 2015; published online on March 24, 2016. Discussion period open until August 24, 2016; separate discussions must be submitted for individual papers. This paper is part of the *Journal of Computing in Civil Engineering*, © ASCE, ISSN 0887-3801.

By contrast to the ease with which  $S$  is computed, the most popular and commonly used measure of roundness ( $R$ ) developed by Wadell (1932, 1933, 1935), does not lend itself to simple image analysis. Wadell defined  $R$  as the ratio of the average radius of curvature of a particle's corners to the radius of the largest possible inscribed circle. In Wadell's original procedure, the particle outline was traced and enlarged to a size of 7.0 cm (2.7 in.). Each corner along the outline was then compared to a set of circle templates in search of the largest circle that would fit it. Obviously, considerable effort was required to evaluate even a small number of particles; a statistically valid sampling was simply unachievable. Nevertheless, Wadell's manual procedure is still occasionally used today when relatively accurate  $R$  values are sought for a small number of particles (Moroto and Ishii 1990; Rouse et al. 2008; Yang and Wei 2012).

To accelerate the estimation of  $R$ , charts containing particle silhouettes of known Wadell  $R$  were developed by Krumbein (1941), Krumbein and Sloss (1951), and Power (1953). Users could quickly estimate  $R$  by observing their particles under a microscope and comparing them to the particles in the standard charts. Although more rapid, this approach is subjective and yields inconsistent results between evaluators. Nevertheless, the chart methods are widely used in a variety of disciplines including geotechnical engineering, soil science, agriculture, powder engineering, pavement engineering, and geology (Eisma 1965; Youd 1973; Frossard 1979; Sladen et al. 1985; Vepraskas and Cassel 1987; Sagga et al. 1993; Vallejo and Zhou 1995; Santamarina and Cho 2004; Mitchell and Soga 2005; Masad et al. 2007; Cho et al. 2006; Mehring and McBride 2007; Bareither et al. 2008; Altuhafi et al. 2013; Chapuis 2012; Shin and Santamarina 2013; Cabalar et al. 2013; Kandasami and Murthy 2014; Oh et al. 2014).

Some researchers have developed alternative roundness descriptors whose parameters could be obtained through digital image analysis. These have included Fourier coefficients (Bowman et al. 2001; Wettimuny and Penumadu 2004; Wang et al. 2005; Mollon and Zhao 2012a, b, 2014), an angularity index (Sukumaran and Ashmawy 2001; Tutumluer and Pan 2008), and a fractal dimension (Arasan et al. 2011; Vallejo 1995; Vallejo and Zhou 1995). However, these alternate definitions of roundness have not prevailed over Wadell's because of the latter's long history and deserved popularity.

In light of the continuing usage of Wadell's  $R$  in research and practice, Zheng and Hryciw (2015) proposed a computational geometry algorithm to automate the computation of Wadell's  $R$ . Their method was tested on two particles from Wadell's original 1935 paper and an additional 20 reference particles from the roundness chart of Krumbein and Sloss (1951). Excellent agreement was found between the computed  $R$  values and the chart values. The present paper further tests the roundness algorithm on another 93 reference particles from published standard charts [81 from Krumbein (1941) and 12 from Powers (1953)]. The paper then extends the algorithm to particles selected and delineated from 13 images of three-dimensional (3D) soil assemblies having various geologic origins.

## Computational Geometry Technique for Wadell Roundness

As previously described, the Wadell procedure requires identification of the particle corners and fitting of circles to them. The procedure is difficult to automate because the number of corners and their curvature vary considerably from particle to particle. Human evaluators readily identify the corners and easily fit corresponding corner circles to them using intuition, experience, and judgment. The other previously mentioned roundness descriptors (Fourier coefficients, angularity index, and a fractal dimension) avoid the complex corner identification process by quantifying the curvature over the entire particle perimeter without placing emphasis on corners. Secondly, digital noise and actual roughness along the particle perimeter must be filtered out prior to computing roundness. The noise and roughness could be easily filtered out by a human operator but is challenging for a computer. Some researchers including Sukumaran and Ashmawy (2001) and Tutumluer and Pan (2008) sought to remove the roughness by discretizing the outline of a particle into an  $N$ -sided polygon. The selected  $N$  value de facto served as the cutoff between what would be defined as angularity and what would be roughness. Sukumaran and Ashmawy (2001) suggested that  $N = 40$  would be appropriate while Tutumluer and Pan (2008) believed  $N = 24$  to be adequate. In reality, a single  $N$  value cannot be applied to all particles;  $N$  should vary depending on each particle's individual angularity and roughness. Another limitation of this  $N$ -approach is that small sharp corners can be missed. As such, this approach is problematic for very angular particles.

The issues described previously were addressed and overcome by Zheng and Hryciw (2015). The noise and roughness are removed from particle perimeters using two statistical techniques: locally weighted scatter plot smoothing (LOESS), and  $K$ -fold cross

validation. The corners on the soil particles are identified through computational geometry. Four main steps are required to compute Wadell's  $R$  from a binary soil particle image.

In Step 1 the maximum inscribed circle is found. The particle perimeter in Fig. 1(b) is obtained by tracing the outline of the binary particle silhouette in Fig. 1(a). For each point inside the soil particle, the minimum distance  $D$  to the particle perimeter is computed, which produces a *Euclidean Distance Map* shown in Fig. 1(c). The point  $C$  having maximum  $D$  is the center of the maximum inscribed circle and  $D$  is its radius as shown in Fig. 1(d).

In Step 2 the roughness on the particle outline is removed. A locally weighted scatter plot smoothing (LOESS) technique (Cleveland and Devlin 1988) and  $K$ -fold cross-validation technique (Efron and Tibshirani 1993) are adopted to estimate a mean surface. The particle perimeter is discretized by polar coordinates  $(\theta, \rho)$  in Fig. 2(a) and plotted in Fig. 2(b). The LOESS and  $K$ -fold cross validation are used to filter out the roughness resulting in a smoothed mean surface, also shown in Fig. 2(b). The two lines are indistinguishable unless the plot is highly magnified as shown by expansion of areas (1) and (2). Then, the mean surface is replotted to generate the new smoothed soil particle outline in Fig. 2(c). It is noted that the LOESS and  $K$ -fold cross validation could also be used to quantify the roughness of soil particles (Zheng and Hryciw 2015). In Step 3 the corners on the particle perimeter are identified. An arbitrary curved segment on the perimeter, such as  $AB$  in Fig. 3(a), could be approximated by the chord  $AB$  in Fig. 3(b). The chord must be short enough so that the divergence of the curve from the chord approximating it does not exceed a predetermined critical value given by  $\delta_0$ . Figs. 3(b and c) show the chord approximations of the curve  $AB$  using a larger and a smaller value of  $\delta_0$  respectively. Clearly, a large  $\delta_0$  will result in missed small corners. The physical meaning and determination of the appropriate  $\delta_0$  value will be discussed shortly. Assuming an appropriate  $\delta_0$  is used, the soil particle in Fig. 3(a) is approximated by line segments connecting key points in Fig. 3(d).

The key points could be either on corners or not, as shown in Fig. 3(d). Only the key points that lie on the corners, hereafter termed *corner points*, will be needed to compute roundness. The straightforward method to identify whether a key point [such as point  $E$  in Fig. 3(d)] is a corner point is as follows. The centroid  $O$  of the soil particle is located as shown in Fig. 3(d). The two nearest key points on each side of  $E$  (points  $C$  and  $D$ ) are connected and a line from  $O$  through  $E$  is constructed. The point  $F$  lies at the intersection of  $CD$  and the line from  $O$  through  $E$ . Then, if  $OE > OF$ , point  $E$  is a corner point, whereas if  $OE < OF$  it is not. This process is repeated for all key points. Only the points

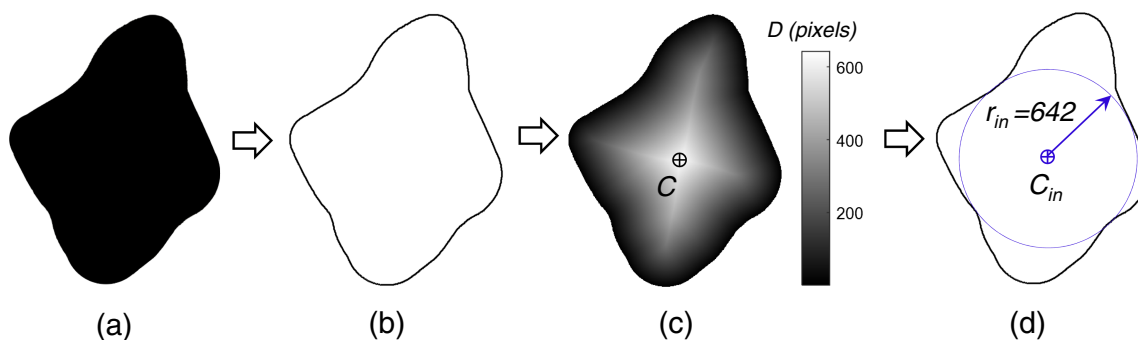


**Fig. 1.** Finding the maximum inscribed circle: (a) the input binary particle image; (b) extracted particle outline; (c) Euclidean distance map; (d) computed maximum inscribed circle

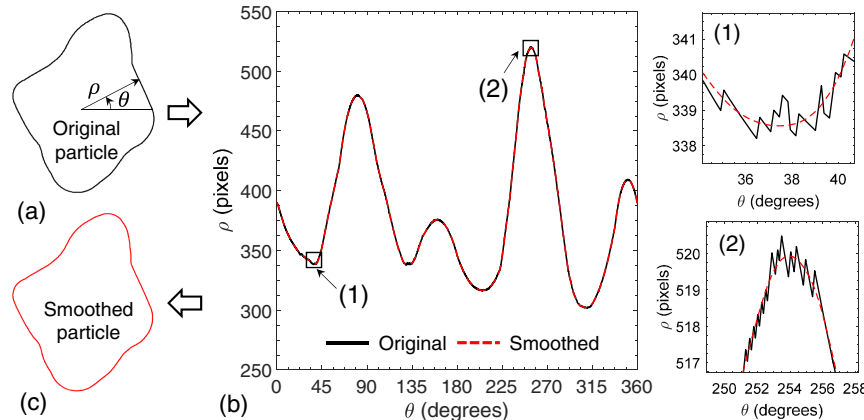


**Fig. 2.** Removing roughness from a particle perimeter: (a) discretization of particle outline using polar coordinates; (b) estimation of particle mean surface; (c) smoothed particle outline

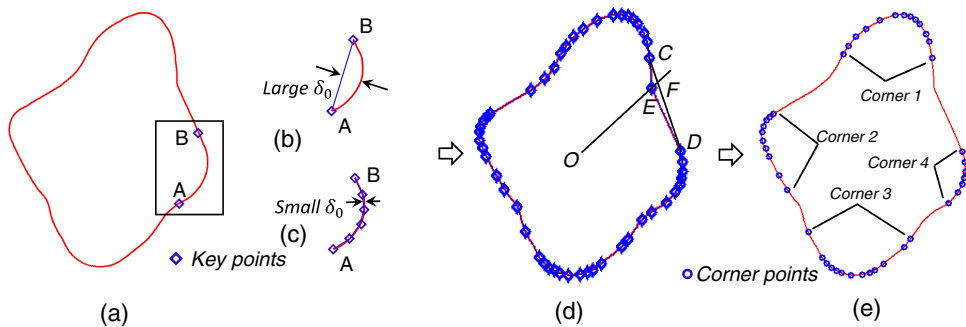


**Fig. 3.** Identifying the corners on the soil particle perimeter: (a) two key point on a particle outline; (b) chord between key points using a large  $\delta_0$ ; (c) chord between key points using a small  $\delta_0$ ; (d) soil particle approximated by line segments connecting key points and the geometry for determining if points are corner points; (e) identified corner points

identified as corner points, 43 in all, are plotted in Fig. 3(e). They reveal four particle corners.

In Step 4 circles are fitted to the corner points as follows. Initially, a large circle is fitted to all 43 corner points as shown in Fig. 4(a). The center of the circle is  $C$  and its radius is  $r$ . The minimum distance from  $C$  to any point on the particle boundary is  $d$ . If  $d$  is smaller than  $r$ , the circle cannot be tangent to the particle boundary. As such, it is not an acceptable circle. If this happens, as it does in Fig. 4(a), the end point 43 is eliminated and point 42 becomes the new last point. Points 1 to 42 are now fitted with a new circle. The recomputed  $d$  and  $r$  values are compared. If  $d$  is still smaller than  $r$ , point 42 is eliminated and 41 becomes the new last point. The process continues until a circle is found satisfying  $d \approx r$  or until only three points are left. Fig. 4(b) shows the last point having moved down to point 22 but still no satisfactory circle was found. Fig. 4(c) shows that the first satisfactory circle was found when the last point moved all the way to point 7. The circle  $C_1$  thus defines the curvature of the first corner. Because points 1 to 7 have now been used to define a corner, in the next loop, the first point moves to point 8 and the last point returns to point 43 as shown in Fig. 4(d).

The previously described process continues with the last point successively moving downward in search of a circle whose  $d \approx r$ . In this loop the last point moved all the way to point 10 without finding an acceptable circle. Thus, the loop ends without an acceptable circle having been found as shown in Fig. 4(e). Because point 8 was not part of any acceptable circle it is eliminated from further

consideration. In the next loop, shown in Fig. 4(f), points 9 to 43 are used in the search for the circle that will fit the second corner. The second proper circle  $C_2$  for which  $d \approx r$  is finally found when the first point is 10 and the last point moves to 19 in Fig. 4(g).

After all the loops are completed and the corner circles are found, a special situation must be checked. The first fitted circle and the last fitted circle may coincide. This happens when point 1 is on a corner, in which case one of the circles containing point 1 is redundant and should be ignored. The final corner circle fitting results are shown in Fig. 4(h). As expected, four circles were found for the four corners. The radii of these circles are then used to compute the average corner radius.

In the previous procedure, the satisfactory circles are found by  $d \approx r$ . However, it is rare that  $d$  is exactly the same as  $r$  due to computational round-off. In fact, Zheng and Hryciw (2015) found that  $0.98 \leq d/r \leq 1.00$  is accurate enough for determining particle roundness.

The last issue is how to determine an appropriate  $\delta_0$ . The value of  $\delta_0$  effectively establishes the threshold between corners and non-corners as shown in Figs. 3(b and c). Therefore,  $\delta_0$  should be set as small as possible to capture all the corners. However, once  $\delta_0$  is smaller than a threshold value by which all the corners are captured, a further decrease in  $\delta_0$  will not improve the results but merely increase computational effort. Zheng and Hryciw (2015) found that a  $\delta_0$  equal to 0.03% of the diameter of the smallest circle that will circumscribe the particle will adequately define the corners of even the most angular particles. To facilitate digital analysis they

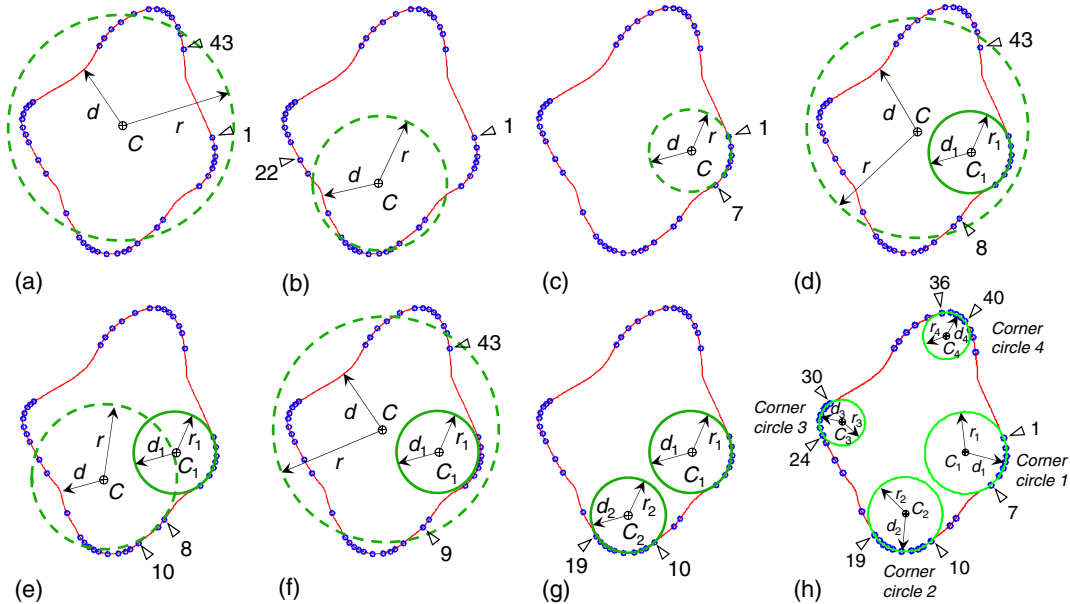


**Fig. 4.** (a–h) Corner circle fitting process as described in the paper

quantified the diameter by the number of pixels per circumscribing circle diameter (PCD). For the particle shown in Figs. 1–4, PCD = 998 pixels as shown in Fig. 5. Therefore,  $\delta_0$  must be at least 0.3 pixels. Another important finding is that the spatial resolution must be set to capture a particle at a PCD of 200 or more. Otherwise, the resolution will not be sufficient to delineate the small corners of very angular particles. Using these criteria, the roundness of the particle shown in Fig. 5 was found to be 0.40.

### Comparison of the Computational Geometry Technique Results with Chart Values of Roundness

The described computational geometry algorithm was previously implemented on 22 particles: 2 particles from Wadell's original 1935 paper and 20 from the Krumbein-Sloss (1951) chart by Zheng and Hryciw (2015). They found excellent agreement between the computed and chart values. In this paper, the algorithm is evaluated

even more comprehensively by comparing its results to roundness charts proposed by Krumbein (1941) and Powers (1953). The Krumbein chart contains 81 reference particles redrawn from pebbles and manually assessed by Wadell's method. As shown in Fig. 6, the 81 reference particles were binned by Krumbein into nine groups having  $R$  increments of 0.1. The authors determined the  $R$  values of all 81 particles using computational geometry. The spatial resolution was set to have a PCD of approximately 1,200 pixels for all of the particles and  $\delta_0$  was set to 0.3 for all computations. The resulting corner circles and maximum inscribed circles are plotted in Fig. 6. The computed  $R$  values are shown with two significant figures over each of the particles in Fig. 6. They are in excellent agreement with the one significant figure values provided by Krumbein (1941) at the bottom of each of the nine groups. When the computational results are rounded to one significant figure, perfect agreement is found for 79 of the 81 particles. The only exceptions are two very well rounded particles that had  $R = 0.97$ , which rounds to 1.0.

It is clear that the computational method furnishes a precise computation of  $R$  whereas the chart methods provide only estimates of it. Indeed, the successful development of the former eliminates the need for the latter.

Another widely used chart for estimating particle sphericity and roundness was provided by Powers (1953). He separated particles having Wadell  $R$  values from 0.12 to 1.00 into six roundness classes as shown in Fig. 7. The ratio of the upper limit to the lower limit of  $R$  in every class is 0.7. Each roundness range is illustrated with two particles: one having high  $S$  and one with low  $S$ . The  $R$  values of the 12 soil particles were determined using the computational methods described in this paper with  $\delta_0$  set to 0.3. The results are shown in Fig. 7. The computed  $R$  values of the two particles in each class are very close to the upper and lower limit in each class. The particles having high  $S$  displayed the upper  $R$  value whereas the particle having low  $S$  displayed the lower  $R$  value in each range. The computed values agree remarkably well with the values reported by Powers (1953). As such, the authors again conclude that the computational geometry method proposed in this paper can replace the imprecise and subjective chart method.

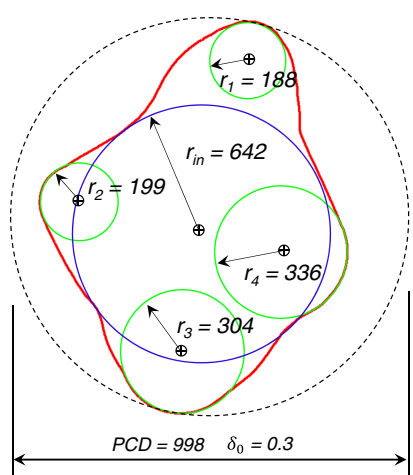


**Fig. 5.** Results of the computational geometry analysis to compute roundness

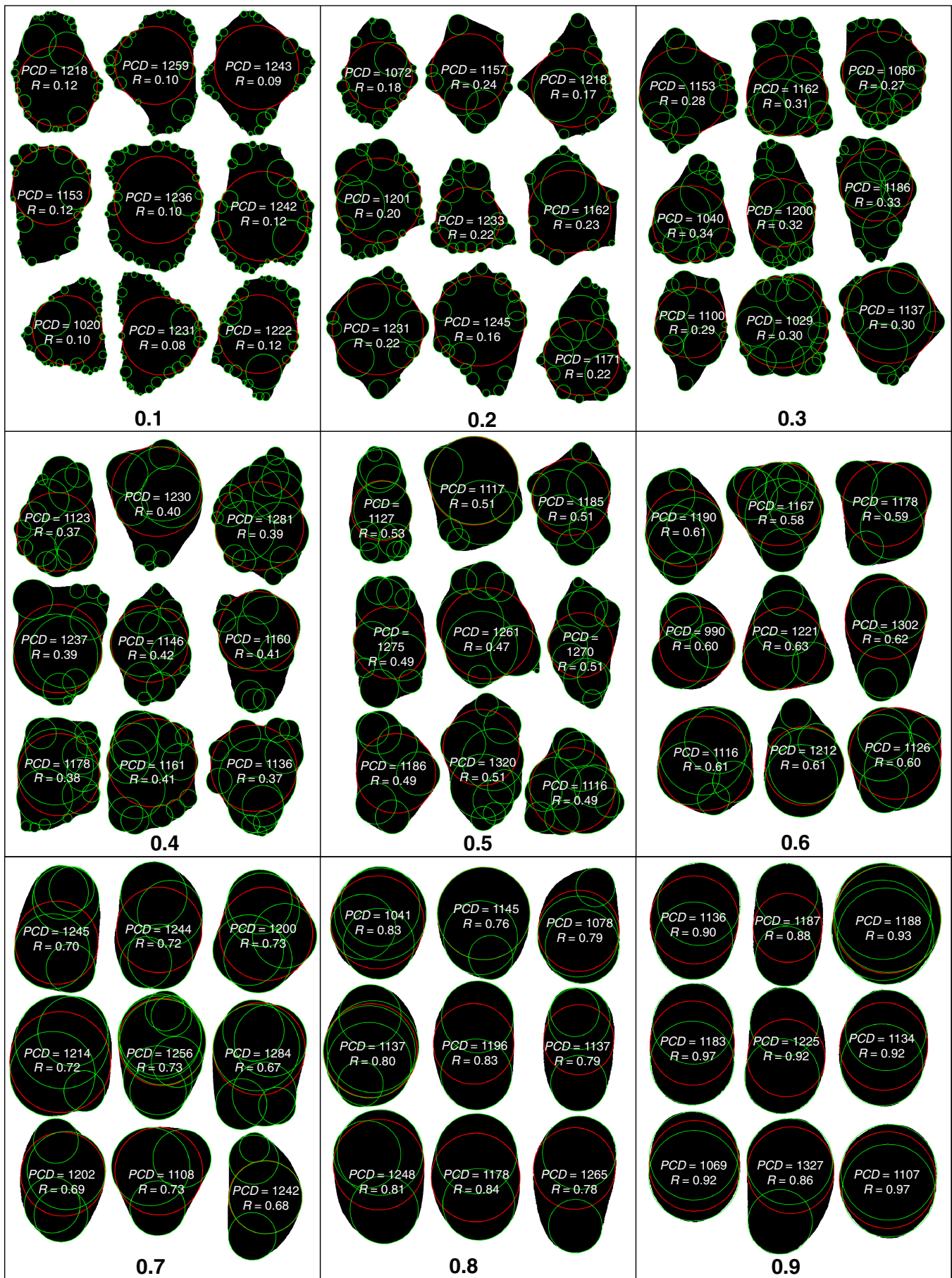


**Fig. 6.** Comparison to results reported by Krumbein (1941) ( $\delta_0 = 0.3$ )

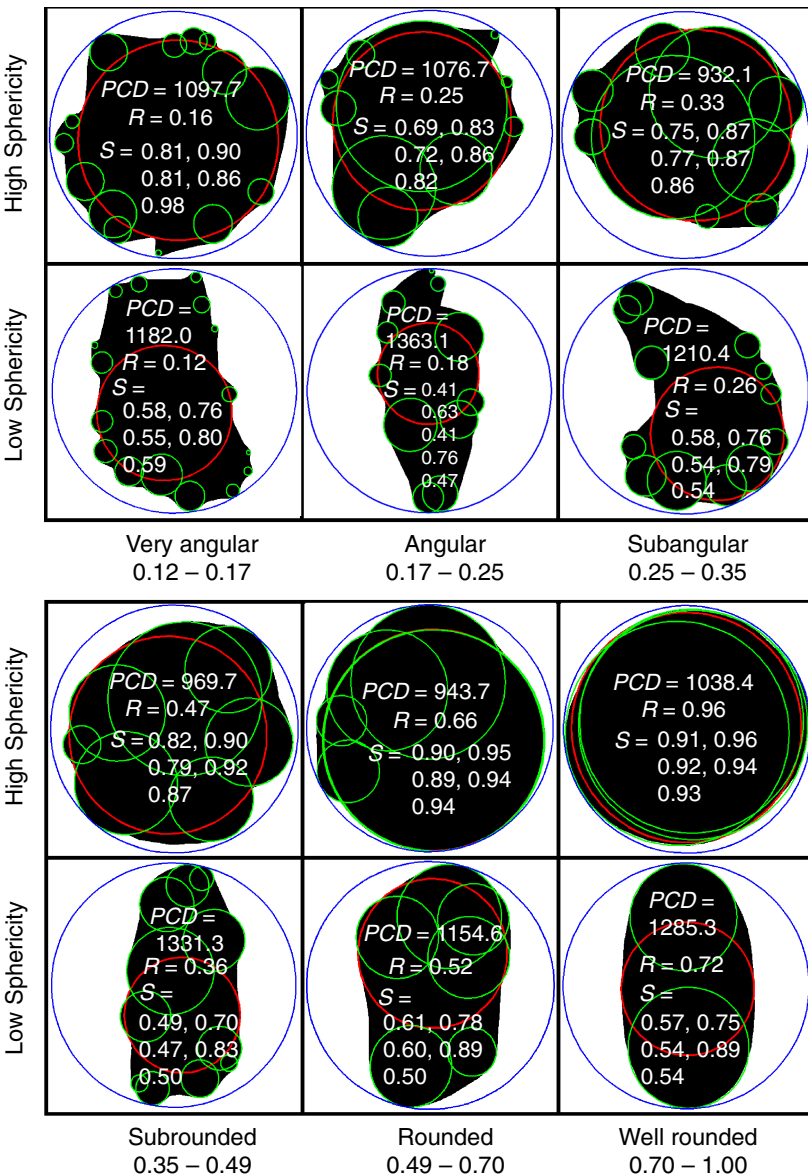


Fig. 7. Comparison of computational method to estimate angularity by Powers (1953)

## Application of the Algorithm to Particle Assemblies

Provided binary particle images, the computational algorithm can directly extract a particle's outline and compute Wadell's  $R$ . Therefore, it could be readily integrated into existing optical soil characterization systems capturing binary soil images. Some of the systems include: the University of Illinois Aggregate Image Analyzer (UIAIA) (Rao and Tutumluer 2000; Tutumluer and Pan 2008); the Aggregate Imaging System (AIMS) (Fletcher et al. 2003; Chandan et al. 2004; Mahmoud and Masad 2007); the Qicpic system (Altuhafi et al. 2013); and the Translucent Segregation Table (TST) system (Ohm and Hryciw 2013). In all of these systems the particles are prepared to lie detached from one another thereby facilitating image collection for simple analysis.

By contrast to the systems listed previously, in other image-based soil characterization systems the soil particles are not or cannot be detached. For example, in the Sedimaging system (Ohm and Hryciw 2013) a 213 cm (7 ft) tall sedimentation column is used to rapidly sort soil particles by size prior to image capture. In these images, the sedimented soil particles are in

three-dimensional contacting assemblies. The Vision Cone Penetrometer (VisCPT) developed by Raschke and Hryciw (1997), Ghalib et al. (2000), Hryciw and Ohm (2013), and Zheng and Hryciw (2015) captures images in situ without taking soil specimens from the ground. Obviously, the soil particles in VisCPT images are also in three-dimensional assemblies. Finally, some particles such as fine sands are so small that it is unrealistic to separate them prior to image capture, even in a laboratory. Therefore, a procedure was sought that could computationally extract particles from images of three-dimensional assemblies so that the new computational algorithm for Wadell's  $R$  could be used on them.

In 3D assemblies, particles are not only in contact with each other, they also block and are blocked from view by other particles. Some soil particles may have a full projection of their area in view while others will be occluded by foreground particles. Secondly, the voids between soil particles are hard to distinguish from actual particles. Naturally, only particles exhibiting full projections are useful for characterization of form and roundness.

Therefore, the challenge is to distinguish particles with full projections from voids and occluded particles. Ideally, a computer

algorithm would make these distinctions. However, this is a daunting task as soils have various colors, size distributions, internal textures, particle forms, and roundnesses. The authors' future research efforts will aim to teach computers to pick out the particles with full projections through machine learning and pattern recognition techniques. However, to date, only human judgment is capable of making the selections. Therefore, a semiautomated approach is used in this paper; it combines human judgment with a computer's rapid computational abilities. In this hybrid approach, operators first pick out the particles with full projections. Then, binary particle images are automatically generated. Finally, roundness and other descriptors of particle geometry are determined using the computational methods described in this paper.

Fig. 8(a) shows a natural soil aggregate image called brown fused alumina oxide sand (BFAO). The particles are brown and have a complex texture. The particles whose projections are fully visible can be manually picked out using the image processing software *Adobe Photoshop*. To begin, the operator can trace the particle boundaries using the *Photoshop* tools polygonal lasso or magnetic lasso. When using the polygonal lasso, users must manually specify the perimeter points and *Photoshop* will connect the points to generate particle boundaries. The magnetic lasso automatically detects the particle boundaries. Although it is a very powerful tool that does not require much human interaction, the magnetic lasso is ineffective for particles that exhibit complex textures because of roughness or mineral variability.

As such, the polygonal lasso was used for the BFAO. A total of 89 fully projected particles were identified. After delineating the boundaries, the regions within them are filled with a distinct color as shown in Fig. 8(b). Fig. 8(b) is the input into the  $R$  computation program previously described. The program easily extracts the newly colored particles and computes the PCD of each one. Each particle is then upscaled or downscaled so that PCD equals 1,000 pixels and  $\delta_0$  is set to 0.3. The results have been superimposed on the original image in Fig. 8(c) and a magnification of the shown rectangular region in Fig. 8(d). The dashed circles are the maximum inscribed circles and the solid circles are corner circles.

Images of two other soils were collected using different optical systems. Fig. 9 shows standard Ottawa #20–#30 sand captured using the VisCPT. The particles are light brown, rounded, and spherical. The soil in Fig. 10 is called 2NS by the Michigan Department of Transportation; an image of its 1.4–2.0 mm size increment was captured in the Sedimaging device. The detailed Sedimaging test procedures are provided by Ohm and Hryciw (2013). The 2NS par-

ticles have a variety of colors, shapes, and roundnesses. In the Ottawa sand image 129 particles showed full projections, whereas 203 particles were found in the 2NS image. The computational results for the two soils are superimposed on the original images. Once again, the maximum inscribed circles are dashed while the corner circles are solid. They again appear to nicely fit the particles and their corners.

## Wadell Roundness and Sphericity Distributions

After identifying the maximum inscribed circle and corner circles, the Wadell  $R$  of each particle is easily computed. Other geometric descriptors such as length ( $d_1$ ), width ( $d_2$ ), sphericity, aspect ratio, orientation can also be readily obtained. Assuming the soil particles are ellipses, a relative volume of each particle can be computed as  $d_1 \times d_2 \times d_3$ . The distribution of Wadell  $R$  by volume for the three soils was computed and is shown in Fig. 11. The use of volume-based distributions for civil engineering (geomechanics) applications is more logical and appropriate than simple distributions based on particle counts. Nevertheless, it's recognized that for relatively uniform sized soil particles the distributions will be similar.

Powers' classification of  $R$  (according to Fig. 7) is also shown in Fig. 11. As shown, the Ottawa sand is 75% by volume well-rounded with about 25% rounded; 2NS contained approximately 45% rounded and 35% subrounded with smaller volumes of well-rounded (10%) and subangular (10%); the BFAO was 50% subangular, 20% angular, and 30% subrounded by volume.

By convention,  $R$  should be evaluated in the view showing the largest projected area of a particle (Sneed and Folk 1958). Therefore, approximately 200 random particles from each of the three sands were laid out on a flat surface exposing their largest area. Images were captured and analyzed using the computational method. The results, shown by dashed lines in Fig. 11 are in very good agreement with those obtained from the images of three-dimensional assemblies. As summarized in Table 1, the difference between the average  $R$  determined from images of assemblies and the average  $R$  from images of detached particles was  $\pm 0.01$  for all three soils.

Having identified particles with full projections, particle sphericities can also be computed and their distributions can also be developed. Sphericity quantifies the similarity of a particles overall shape (form) to a perfect circle or sphere. Over the years, at least five different definitions have been used to quantify  $S$

$$\text{Area Sphericity: } S_A = \frac{\text{Area of soil particle}}{\text{Area of minimum circumscribed circle}} \quad (1)$$

$$\text{Diameter Sphericity: } S_D = \frac{\text{Diameter of circle with same area of soil particle}}{\text{Diameter of minimum circumscribed circle}} \quad (2)$$

$$\text{Circle Ratio Sphericity: } S_C = \frac{\text{Diameter of maximum inscribed circle}}{\text{Diameter of minimum circumscribed circle}} \quad (3)$$

$$\text{Perimeter Sphericity: } S_P = \frac{\text{Perimeter of circle with same area of soil particle}}{\text{Perimeter of soil particle}} \quad (4)$$

$$\text{Width to Length Ratio Sphericity: } S_{WL} = \frac{\text{Width of soil particle}}{\text{Length of soil particle}} \quad (5)$$

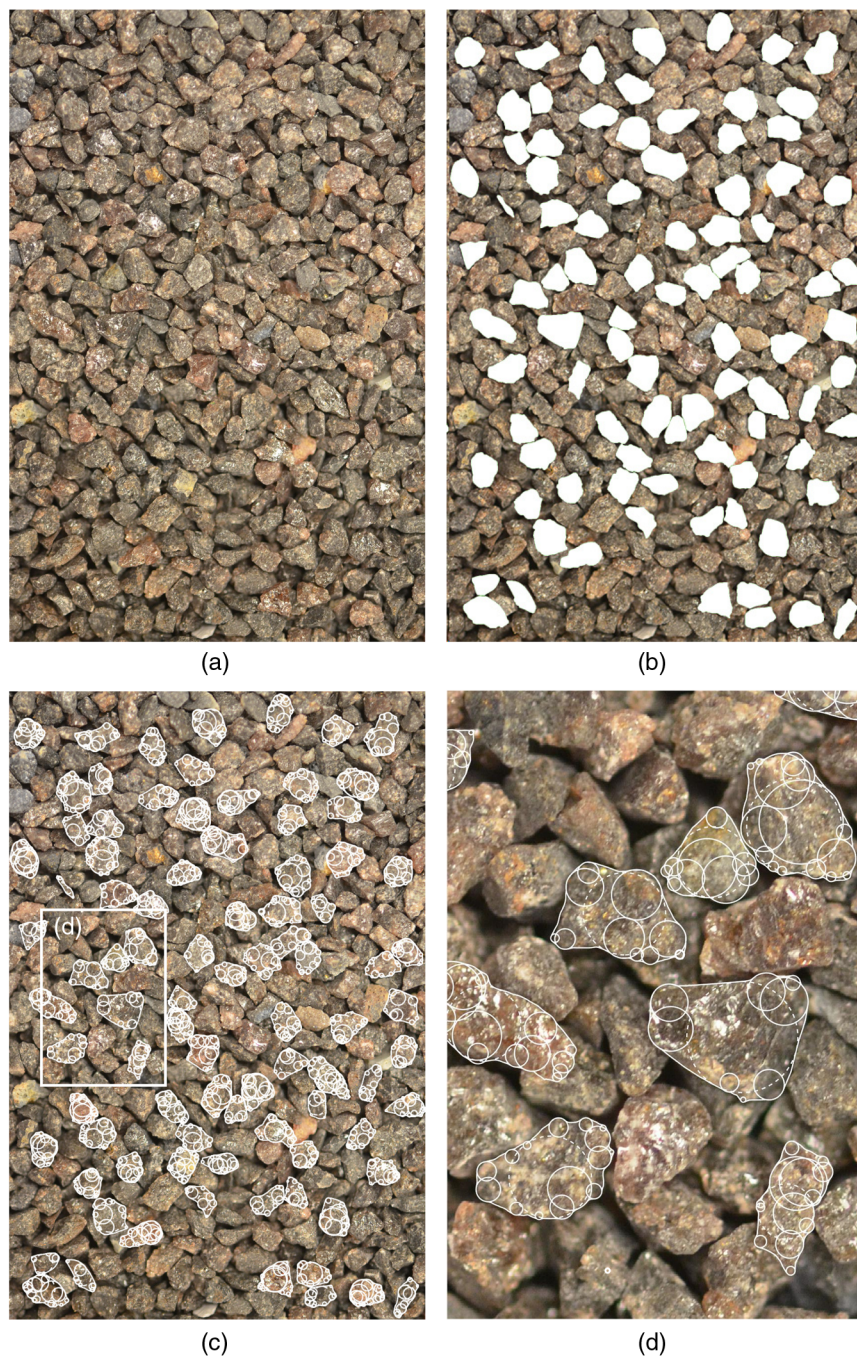


**Fig. 8.** Circle fitting results for BFAO sand: (a) image of the three-dimensional assembly of BFAO; (b) delineated particles using *Photoshop* polygonal lasso tool; (c and d) fitted corner circles (solid) and maximum inscribed circles (dashed)

Eqs. (1)–(5) were either proposed or have been adapted from Tickell (1931), Wadell (1935), Santamarina and Cho (2004), Altuhafi et al. (2013), Krumbein and Sloss (1951, 1963), respectively. Sphericity values by all five definitions are shown for comparison for the particles in Fig. 7. Zheng and Hryciw (2015) reviewed the origins of the five equations, presented their computational methods, and extensively compared their effectiveness at quantifying sphericity by two criteria: (1) their abilities to discriminate sphericity (displaying a significant numerical range for particles for angular to rounded particles); and (2) being unaffected by the roundness of soil particles. The study showed that  $S_{WL}$  is the ideal definition for  $S$  as it best satisfies both criteria.

Nevertheless, for comparison, all five sphericities were computed for the three soils. Figs. 12(a–c) are the  $S$  distributions

for BFAO, Ottawa #20–#30, and 2NS, respectively. The results confirm that  $S_{WL}$  indeed gives a widest numerical range for  $S$ . The dashed lines in the three figures are the  $S$  distributions obtained using the largest projected areas of the same particles as were used for computing roundness. The average values for all three soils by all five definitions of  $S$  are listed in Table 1. As observed, the differences in average values were at most  $\pm 0.02$ .

#### Required Sample Size for Determining Particle Roundness of a Soil

In most earlier studies only a mean  $R$  value for a soil was determined. The ability to rapidly determine  $R$  for numerous particles

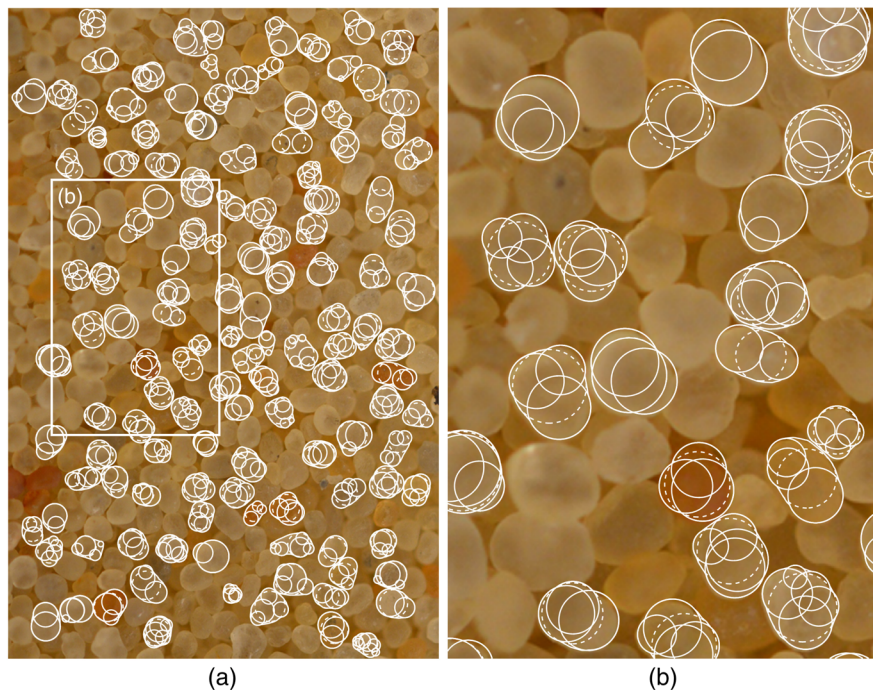


**Fig. 9.** Circle fitting results for Ottawa #20–#30: (a) image of the three-dimensional assembly of Ottawa #20–#30 by VisCPT; (b) fitted corner circles (solid) and maximum inscribed circles (dashed)

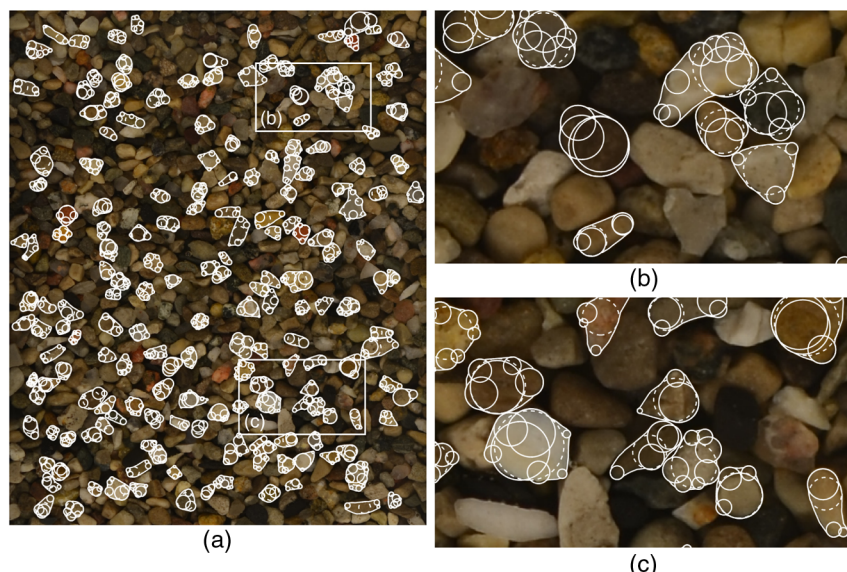


**Fig. 10.** Circle fitting results for 2NS sand: (a) image of a three-dimensional assembly of 2NS sand by sedimaging; (b and c) fitted corner circles (solid) and maximum inscribed circles (dashed)

in a specimen raises the question of how many are needed to obtain statistically valid value. To obtain an average  $R$  for a soil specimen, Youd (1973) reported that at least 50 particles are needed. Edil et al. (1975) estimated  $R$  for sand particles by Krumbein's chart and reported that viewing at least 25 particles were needed to yield a reliable mean. Cho et al. (2006) visually compared 30 particles to obtain the mean. Rouse et al. (2008) concluded that at least 30 particles are needed to compute the mean  $R$  based on the probability theorem law of large numbers. Bareither et al. (2008) used

50 particles. Cavarretta et al. (2010) believed that examining 30–40 particles would be adequate. Yang and Wei (2012) reported using 40 particles. Others who computed and reported average  $R$  values include Eisma (1965), Frossard (1979), Sladen et al. (1985), Vepraskas and Casselkan (1987), Sagga et al. (1993), Frossard (1979), Mehring and McBride (2007), Bareither et al. (2008), Chapuis (2012), and Cabalar et al. (2013). In summary, the typical sample size used to compute an average  $R$  value has been in the range of 30–50 particles.

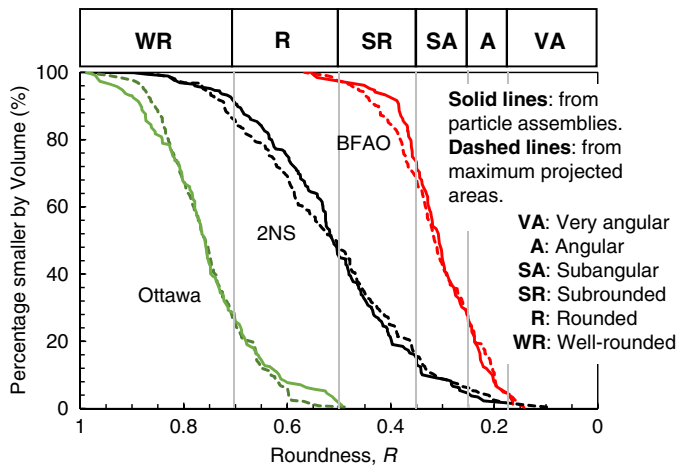


**Fig. 11.** Wadell roundness cumulative distributions

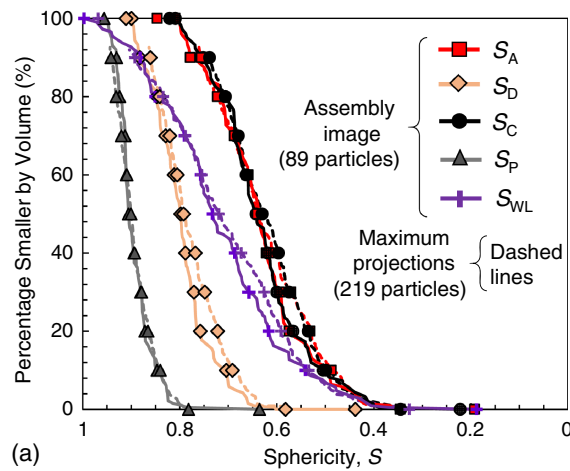
From statistics, for normal distributions the minimum sample size,  $n_{\min}$  necessary for reliably estimating the mean value of a population is computed by

$$n_{\min} = \left[ \frac{z_{\alpha/2}\sigma}{E} \right]^2 \quad (6)$$

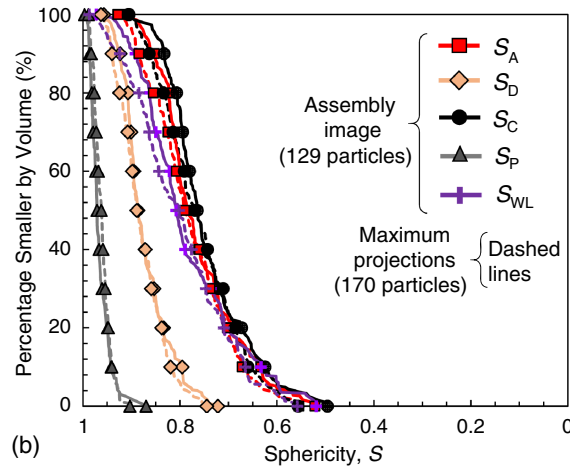
where  $E$  = allowed error between the estimated population mean and the actual population mean;  $\sigma$  = population standard deviation; and  $Z_{\alpha/2}$  = value related to the confidence level of  $100(1 - \alpha)\%$ , which is obtained from a Z-table.

If a maximum  $E$  of 0.05 is established for the mean roundness with a confidence level of 98%, then  $\alpha = 0.02$  and  $Z_{\alpha/2} = Z_{0.01} = 2.33$  from the Z-table. From study of over 20 different sands, the authors have observed standard deviations of no more than 0.17 for roundness, with most values below 0.15. Using the worst case  $\sigma = 0.17$  with  $E = 0.05$  and a 98% desired confidence ( $\alpha = 0.02$ ), the computed  $n_{\min}$  is 63. Because this paper presents a more rapid and precise method for computing roundness than by chart methods it is also logical that more particles could and should be used than the previously used 30–50.

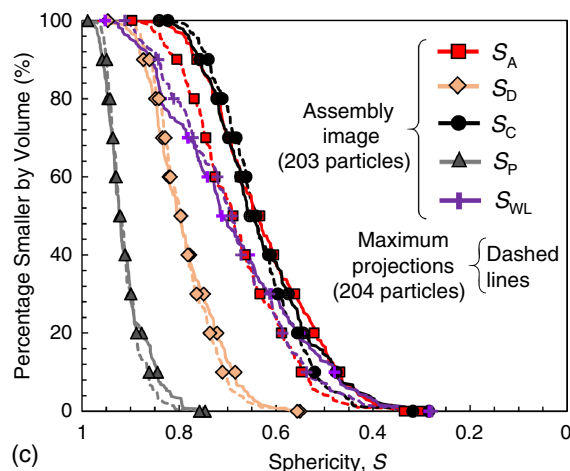
Eight natural and two crushed sands from various locations in Michigan, Texas, Missouri, New Mexico, and California having various particle shapes were evaluated using the computational geometry methods for  $R$  and  $S$ . In each case, the average value of 64 particles was computed. The mean  $R$  values with their standard deviations and the mean  $S_{WL}$  with their standard deviations are shown in Fig. 13. As expected, the two crushed sands, 30A ( $R = 0.15$ ) and a crushed gabbro rock ( $R = 0.23$ ) were the most angular, as expected. Fort Davis, Texas ( $R = 0.41$ ) is very recent colluvium. Scotts Valley, California ( $R = 0.40$ ) is a residual sand from a mildly cemented sandstone. Rincon, New Mexico



(a)



(b)



(c)

**Fig. 12.** Sphericity distributions for (a) BFAO; (b) Ottawa #20-#30; (c) 2NS

**Table 1.** Mean  $R$  and  $S$  from Images of Assemblies and Images of Maximum Area Projections

Soil	$R$		$S_A$		$S_D$		$S_C$		$S_P$		$S_{WL}$	
	IA	MP	IA	MP	IA	MP	IA	MP	IA	MP	IA	MP
BFAO	0.31	0.32	0.62	0.62	0.78	0.78	0.62	0.62	0.88	0.89	0.69	0.70
Ottawa	0.75	0.76	0.75	0.77	0.87	0.88	0.74	0.76	0.96	0.96	0.79	0.80
2NS	0.53	0.52	0.62	0.64	0.78	0.79	0.62	0.63	0.91	0.92	0.67	0.67

Note: IA = from images of assemblies; MP = from images of maximum area projections.

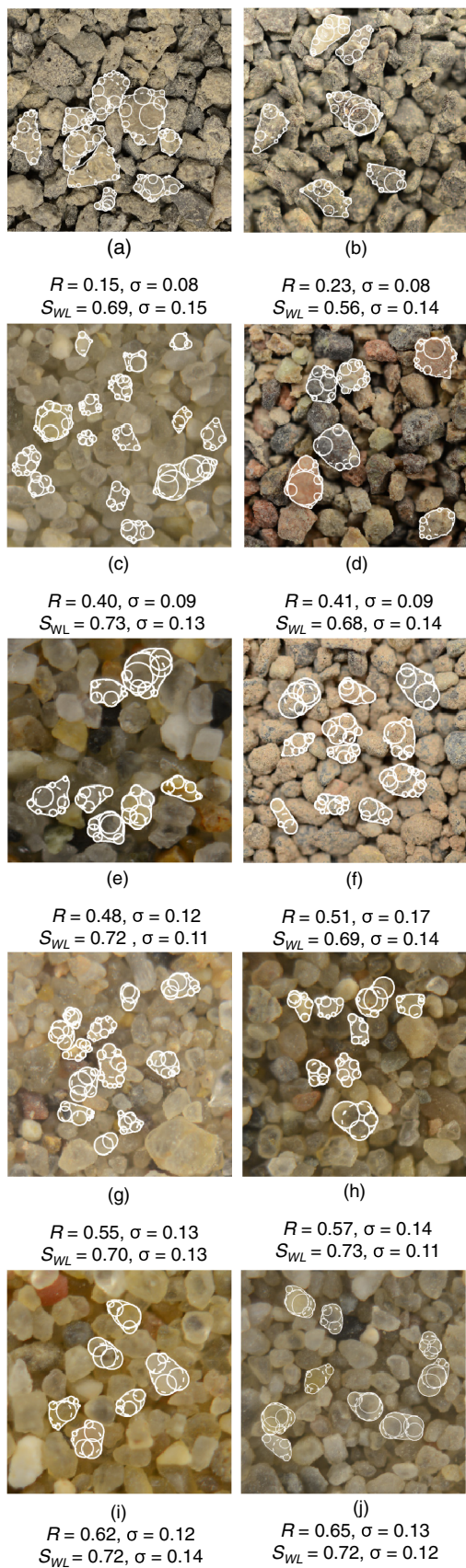


**Fig. 13.** Mean  $R$  and  $S$  values and their standard deviations for sands of various geologic origins: (a) Michigan 30A; (b) Crushed Gabbro; (c) Scotts Valley, California; (d) Fort Davis, Texas; (e) Capitola, California; (f) Upper Peninsula, Michigan; (g) Rincon, New Mexico; (h) New Madrid, Missouri; (i) Lake Michigan Dunes; (j) Oakland County, Michigan

( $R = 0.55$ ) is a dessert sand, probably windblown. Capitola, California ( $R = 0.48$ ) is an alluvial river bed sand. The most rounded soils are a Mississippi River alluvium from New Madrid, Missouri ( $R = 0.57$ ); a glaciofluvial sand from Oakland County, Michigan ( $R = 0.65$ ); and a Lake Michigan Dune sand ( $R = 0.62$ ).

Visual observation of the images appears to confirm the reasonableness of the  $R$  values and classifications. Just as importantly, the inscribed circles and circles fitted to corners are correctly constructed. The largest observed standard deviation was 0.17 confirming the reasonableness of using  $\sigma = 0.17$  in Eq. (1) to compute  $n_{\min}$ .

## Discussion and Future Studies

Mean particle roundness has been correlated to various soil properties including minimum and maximum packing densities, the angle of internal friction, critical state soil parameters, and compressibility. No attempts have been made to relate such properties to distributions of particle  $R$  and  $S$  such as shown in Figs. 11 and 12. Although such research is yet to be performed, it is worth considering what number of particles is needed to yield a statistically valid distribution of  $R$ . If the  $R$  values exhibit a normal distribution, an empirical rule of thumb used by many statisticians suggests that only 30 samples are sufficient to produce the distribution. Intuitively, soils with larger standard deviations and longer tails on the ends of the distribution curves should require more samples. Of course, non-normal distributions would require a larger number of samples. It is also noted that sampling bias could outweigh the considerations of adequate sample size.

Finally, the soil specimens used in this study consisted of relatively uniform-sized particles. Real soils, particularly if engineered for foundations, pavement subbases and other fills are typically better graded. Additional study is needed to evaluate how  $R$  and  $S$  values could vary with the size of particles in such sands.

## Conclusions

A computational geometry method was recently developed to determine soil particle roundness and sphericity by their traditional definitions developed in the 1930s by Hakon Wadell. In this paper, the computed values were compared to visual charts of particle  $R$  and  $S$  developed in the 1950s. The agreement was excellent and given that the computational method is rapid and nonsubjective, it should eliminate the need for usage of such charts, except possibly as a qualitative visual guide.

In this paper, the computational geometry methods were extended to particles in three-dimensional assemblies that exhibited full and unobscured projections. For particles exhibiting uniform internal textures, *Photoshop*'s magnetic lasso tool was used to define the perimeter, whereas for particles with complex internal textures *Photoshop*'s polygonal lasso was used. Cumulative volume-based distribution of particle roundness and sphericity were developed for uniformly textured Ottawa sand and Michigan 2NS as well as for a highly textured brown fused aluminum oxide sand (BFAO). As expected, the Ottawa sand proved to be mostly well-rounded (75%) with about 25% by volume rounded particle; 2NS ranged from 35% subrounded to 45% rounded with smaller volumes of well-rounded (10%) and subangular particles (10%); the BFAO was 50% subangular, 20% angular, and 30% subrounded. Sphericity distributions for these three soils confirmed that the ratio of particle width to length [as sphericity was defined by Krumbein and Sloss (1963)] provides a broader range of values

than four other occasionally used definitions of sphericity. Average values of  $R$  and  $S$  obtained from the images of three-dimensional assemblies were also compared to average values obtained from images of detached particles of the same sands laid out to expose their largest projected areas. The differences in computed  $R$  and  $S$  were insignificant.

Finally, mean  $R$  was computed for 10 different sands of various geologic origins. Their values ranged from 0.15 and 0.25 for crushed sands to 0.40–0.65 for alluvial and glacio-fluvial sands. It was shown that 64 particles were adequate to compute a mean roundness with  $\pm 0.05$  accuracy and 98% confidence.

## Acknowledgments

This material is based upon work supported by the U.S. National Science Foundation under Grant No. CMMI 1300010. ConeTec Investigations Ltd. and the ConeTec Education Foundation are acknowledged for their support to the Geotechnical Engineering Laboratories at the University of Michigan.

## Notation

The following symbols are used in this paper:

- $d_1$  = length of a particle;
- $d_2$  = width of a particle;
- $E$  = the allowed error between the estimated population mean and the actual population mean;
- $n_{\min}$  = the minimum sampling number for estimating population mean;
- PCD = pixels per circumscribing circle diameter;
- $R$  = roundness;
- $S$  = sphericity;
- $Z_{\alpha/2}$  = value related to the confidence level of  $100(1 - \alpha)\%$ , which is obtained from a Z-table;
- $\delta_0$  = maximum allowed divergence of a curve from the straight line segment approximating it;
- $\theta$  and  $\rho$  = polar coordinates; and
- $\sigma$  = the population standard deviation.

## References

- Altuhafi, F., O'Sullivan, C., and Cavaretta, I. (2013). "Analysis of an image-based method to quantify the size and shape of sand particles." *J. Geotech. Geoenviron. Eng.*, **10.1061/(ASCE)GT.1943-5606.0000855**, 1290–1307.
- Arasan, S., Akbulut, S., and Hasiloglu, A. S. (2011). "The relationship between the fractal dimension and shape properties of particles." *KSCE J. Civ. Eng.*, **15**(7), 1219–1225.
- Bareither, C. A., Edil, T. B., Benson, C. H., and Mickelson, D. M. (2008). "Geological and physical factors affecting the friction angle of compacted sands." *J. Geotech. Geoenviron. Eng.*, **10.1061/(ASCE)1090-0241(2008)134:10(1476)**, 1476–1489.
- Bowman, E. T., Soga, K., and Drummond, W. (2001). "Particle shape characterization using Fourier descriptor analysis." *Géotechnique*, **51**(6), 545–554.
- Cabalar, A. F., Dulundu, K., and Tuncay, K. (2013). "Strength of various sands in triaxial and cyclic direct shear tests." *Eng. Geol.*, **156**(1), 92–102.
- Cavaretta, I., O'Sullivan, C., and Coop, M. (2010). "The influence of particle characteristics on the behaviour of coarse grained soils." *Géotechnique*, **60**(6), 413–423.
- Chandan, C., Sivakumar, K., Masad, E., and Fletcher, T. (2004). "Application of imaging techniques to geometry analysis of aggregate particles." *J. Comput. Civ. Eng.*, **10.1061/(ASCE)0887-3801(2004)18:1(75)**, 75–82.
- Chapuis, R. P. (2012). "Estimating the in situ porosity of sandy soils sampled in boreholes." *Eng. Geol.*, **141–142**(19), 57–64.
- Cho, G. C., Dodds, J., and Santamarina, C. (2006). "Particle shape effects on packing density, stiffness, and strength: Natural and crushed sands." *J. Geotech. Geoenviron. Eng.*, **10.1061/(ASCE)1090-0241(2006)132:5(591)**, 591–602.
- Cleveland, W. S., and Devlin, S. J. (1988). "Locally weighted regression: An approach to regression analysis by local fitting." *J. Am. Stat. Assoc.*, **83**(403), 596–610.
- Edil, T. B., Krizek, R. J., and Zelasko, J. S. (1975). "Effect of grain characteristics on packing of sands." *Proc., of Istanbul Conf. on Soil Mechanics and Foundation Engineering*, Istanbul Technical Univ., Istanbul, Turkey, 46–54.
- Efron, B., and Tibshirani, R. J. (1993). *An introduction to the bootstrap*, Chapman and Hall/CRC, New York.
- Eisma, D. (1965). "Eolian sorting and roundness of beach and dune sands." *Neth. J. Sea Res.*, **2**(4), 541–555.
- Fletcher, T., Chandan, C., Masad, E., and Sivakumar, K. (2003). "Aggregate imaging system for characterizing the shape of fine and coarse aggregates." *Transp. Res. Rec.*, **1832**, 67–77.
- Frossard, E. (1979). "Effect of sand grain shape on the interparticle friction; indirect measurements by Rowe's stress dilatancy theory." *Géotechnique*, **29**(3), 341–350.
- Ghalib, A. M., Hryciw, R. D., and Susila, E. (2000). "Soil stratigraphy delineation by VisCPT." *Innovations and Applications in Geotechnical Site Characterization*, ASCE, Reston, VA, 65–79.
- Hryciw, D. R., Zheng, J., Ohm, H., and Li, J. (2014). "Innovations in optical geocharacterization." *Geo-Congress 2014 Keynote Lectures: Geo-Characterization and Modeling for Sustainability*, Vol. 235, ASCE, Reston, VA, 97–116.
- Hryciw, R. D. and Ohm, H.-S. (2013). "Soil migration and piping susceptibility by the VisCPT." *Geo-Congress 2013: Stability and Performance of Slopes and Embankments III*, ASCE, Reston, VA, 192–195.
- Kandasami, R. K., and Murthy, T. G. (2014). "Effect of particle shape on the mechanical response of a granular ensemble." *Proc., Int. Symp. on Geomechanics from Micro to Macro*, Taylor & Francis Group, Boca Raton, FL, 1093–1098.
- Krumbein, W. C. (1941). "Measurement and geological significance of shape and roundness of sedimentary particles." *J. Sediment. Petrol.*, **11**(2), 64–72.
- Krumbein, W. C., and Sloss, L. L. (1951). *Stratigraphy and sedimentation*, W. H. Freeman and Company, San Francisco.
- Krumbein, W. C., and Sloss, L. L. (1963). *Stratigraphy and sedimentation*, 2nd Ed., W. H. Freeman and Company, San Francisco.
- Kumara, G. J. J., Hayano, K., and Ogiwara, K. (2012). "Image analysis techniques on evaluation of particle size distribution of gravel." *Int. J. Geomate.*, **3**(1), 290–297.
- Kuo, C. Y., and Freeman, R. B. (2000). "Imaging indices for quantification of shape, angularity and surface texture of aggregates." *Transp. Res. Rec.*, **1721**, 57–65.
- Kuo, C. Y., Frost, J. D., Lai, J. S., and Wang, L. B. (1996). "Three-dimensional image analysis of aggregate particles from orthogonal projections." *Transp. Res. Rec.*, **1526**, 98–103.
- Mahmoud, E., and Masad, E. (2007). "Experimental methods for the evaluation of aggregate resistance to polishing, abrasion, and breakage." *J. Mater. Civ. Eng.*, **10.1061/(ASCE)0899-1561(2007)19:11(977)**, 977–985.
- Masad, E., Al-Rousan, T., Button, J., Little, D., and Tutumluer, E. (2007). "Test methods for characterizing aggregate shape, texture, and angularity." *National Cooperative Highway Research Program Rep. No. 555*, Transportation Research Board, Washington, DC.
- Mehring, J. L., and McBride, E. F. (2007). "Origin of modern quartzarenite beach sands in a temperate climate, Florida and Alabama, USA." *Sed. Geol.*, **201**(3–4), 432–445.
- Mitchell, J. K., and Soga, K. (2005). *Fundamentals of soil behavior*, 3rd Ed., Wiley, New York.

- Mollon, G., and Zhao, J. D. (2012a). "Fourier-Voronoi-based generation of realistic samples for discrete modelling of granular materials." *Granular Matter*, 14(5), 621–638.
- Mollon, G., and Zhao, J. D. (2012b). "Generating realistic 3D sand particles using Fourier descriptors." *Granular Matter*, 15(1), 95–108.
- Mollon, G., and Zhao, J. D. (2014). "3D generation of realistic granular samples based on random fields theory and Fourier shape descriptors." *Comput. Meth. Appl. Mech. Eng.*, 279, 46–65.
- Moroto, N., and Ishii, T. (1990). "Shear strength of uni-sized gravels under triaxial compression." *Soils Found.*, 30(2), 23–32.
- Oh, T. M., Joo, G. W., Yun, K. J., and Cho, G. C. (2014). "Crush characteristics of abrasive particles during abrasive waterjet rock cutting." *Proc., Int. Symp. on Geomechanics from Micro to Macro*, Taylor & Francis Group, Boca Raton, FL, 1577–1581.
- Ohm, H. S., and Hryciw, R. D. (2013). "Translucent segregation table test for sand and gravel particle size distribution." *Geotech. Test. J.*, 36(4), 592–605.
- Powers, M. C. (1953). "A new roundness scale for sedimentary particles." *J. Sediment. Petrol.*, 23(2), 117–119.
- Rao, C., and Tutumluer, E. (2000). "Determination of volume of aggregates." *Transp. Res. Rec.*, 1721, 73–80.
- Raschke, S., and Hryciw, R. (1997). "Vision cone penetrometer for direct subsurface soil observation." *J. Geotech. Geoenviron. Eng.*, 10.1061/(ASCE)1090-0241(1997)123:11(1074), 1074–1076.
- Rouse, P. C., Fannin, R. J., and Shuttle, D. A. (2008). "Influence of roundness on the void ratio and strength of uniform sand." *Géotechnique*, 58(3), 227–231.
- Sagga, M. A. (1993). "Roundness of sand grains of longitudinal dunes in Saudi Arabia." *Sediment. Geol.*, 87(1–2), 63–68.
- Santamarina, J. C., and Cho, G. C. (2004). "Soil behaviour: The role of particle shape." *Advances in Geotechnical Engineering: The Skempton Conf.*, Thomas Telford, London, 604–617.
- Shin, H., and Santamarina, J. C. (2013). "The role of particle angularity on the mechanical behavior of granular mixtures." *J. Geotech. Geoenviron. Eng.*, 10.1061/(ASCE)GT.1943-5606.0000768, 353–355.
- Sladen, J. A., D'Hollander, R. D., and Krahn, J. (1985). "The liquefaction of sands, a collapse surface approach." *Can. Geotech. J.*, 22(4), 564–578.
- Sneed, E. D. and Folk, R. L. (1958). "Pebbles in the lower Colorado River, Texas: A study of particle morphogenesis." *J. Geol.*, 66(2), 114–150.
- Sukumaran, B., and Ashmawy, A. K. (2001). "Quantitative characterization of the geometry of discrete particles." *Géotechnique*, 51(7), 619–627.
- Tickell, F. G. (1931). *The examination of fragmental rocks*, Stanford University Press, Stanford, CA.
- Tutumluer, E., and Pan, T. (2008). "Aggregate morphology affecting strength and permanent deformation behavior of unbound aggregate materials." *J. Mater. Civ. Eng.*, 10.1061/(ASCE)0899-1561(2008)20:9(617), 617–627.
- Vallejo, L. E. (1995). "Fractal analysis of granular materials." *Géotechnique*, 45(1), 159–163.
- Vallejo, L. E., and Zhou, Y. (1995). "The relationship between the fractal dimension and Krumbein's roundness number." *Soils Found.*, 35(1), 163–167.
- Vepraskas, M. J., and Cassel, D. K. (1987). "Sphericity and roundness of sand in coastal plain soils and relationships with soil physical properties." *Soil Sci. Soc. Am. J.*, 51(5), 1108–1112.
- Wadell, H. (1932). "Volume, shape and roundness of rock particles." *J. Geol.*, 40(5), 443–451.
- Wadell, H. (1933). "Sphericity and roundness of rock particles." *J. Geol.*, 41(3), 310–331.
- Wadell, H. (1935). "Volume, shape, and roundness of quartz particles." *J. Geol.*, 43(3), 250–280.
- Wang, L., Wang, X., Mohammad, L., and Abadie, C. (2005). "A unified method to quantify aggregate shape angularity and texture using Fourier analysis." *J. Mater. Civ. Eng.*, 10.1061/(ASCE)0899-1561(2005)17:5(498), 498–504.
- Wettimuny, R., and Penumadu, D. (2004). "Application of Fourier analysis to digital imaging for particle shape analysis." *J. Comput. Civ. Eng.*, 10.1061/(ASCE)0887-3801(2004)18:1(2), 2–9.
- Yang, J., and Wei, L. M. (2012). "Collapse of loose sand with the addition of fines: The role of particle shape." *Géotechnique*, 62(12), 1111–1125.
- Youd, T. L. (1973). "Factors controlling maximum and minimum densities of sands." *Evaluation of relative density and its role in geotechnical projects involving cohesionless soils*, STP 523, ASTM, Philadelphia, 98–112.
- Zheng, J., and Hryciw, R. D. (2015). "Traditional soil particle sphericity, roundness and surface roughness by computational geometry." *Géotechnique*, 65(6), 494–506.